Sh2-205 – II. Quiescent star-formation activity

G. A. Romero[1,2,3]★† and C. E. Cappa[2,3]‡

[1]*Departamento de Física y Astronomía, Universidad de Valparaíso, Avenida Gran Bretaña 1111, Valparaíso, Chile*
[2]*Instituto Argentino de Radioastronomía, CCT-La Plata, CONICET, CC 5, 1894 Villa Elisa, Argentina*
[3]*Facultad de Ciencias Astronómicas y Geofísicas, Universidad Nacional de La Plata, Paseo del Bosque s/n, 1900 La Plata, Argentina*

ABSTRACT

We present a study of active star-forming regions in the environs of the H II region Sh2-205. The analysis is based on data obtained from point source catalogues and images extracted from the Two-Micron All-Sky Survey (2MASS), *Midcourse Space Experiment* (*MSX*) and *IRAS* surveys. Complementary data are taken from a CO survey. The identification of primary candidates for star-formation activity is made following colour criteria and a correlation with molecular gas emission.

A number of star-formation tracer candidates are projected on to two substructures of the H II region: SH 148.83–0.67 and SH 149.25–0.00. However, the lack of molecular gas related to these structures casts doubt on the nature of the sources. Additional infrared sources may be associated with the H I shell centred at $(l, b) = (149°0', -1°30')$.

The most striking active area was found in connection with the H II region LBN 148.11–0.45, where star-formation candidates are projected on to molecular gas. The analytical model of the 'collect and collapse' process shows that star-formation activity could have been triggered by the expansion of this H II region.

Key words: stars: formation – H II regions – ISM: structure – infrared: ISM – infrared: stars.

1 INTRODUCTION

Observational studies have shown that expanding H II regions and interstellar bubbles are surrounded by massive and dense slowly expanding shells. Star formation may be favoured within these dense envelopes around H II regions (Deharveng, Zavagno & Caplan 2005) and stellar wind bubbles through the *collect and collapse* mechanism first described by Elmegreen & Lada (1977), which was analytically developed by Whitworth et al. (1994). Numerical simulations were performed by Dale, Bonnell & Whitworth (2007). In H II regions, this process can be summarized as follows. The supersonic expansion of an H II region relative to its surroundings creates compressed layers where gas and dust are piled up between the ionization and shock fronts. This shocked material grows in mass and may become gravitationally unstable. Under these conditions, the dense envelopes may break up, forming massive cores that could become nurseries for new generations of massive stars. Thus, the dynamical evolution of H II regions provides the conditions for the star-formation process to develop (Deharveng et al. 2003; Zavagno et al. 2006).

A similar process may act in the dense envelopes around interstellar bubbles. Indeed, young stellar object (YSO) candidates have been found projected on to the neutral shells associated with some wind bubbles (e.g. Cappa et al. 2005).

In a previous paper, we studied the interstellar medium (ISM) in the environs of Sh2-205, located at a distance of ~1 kpc (Romero & Cappa 2008, hereinafter referred to as Paper I). In that work, we showed the presence of three independent optical nebulae: SH 149.25–0.00, SH 148.83–0.67 and LBN 148.11–0.45, and an H I shell centred at $(l, b) = (149°0', -1°30')$. For the sake of clarity, the areas discussed in the paper are indicated in Fig. 1. We determined that SH 148.83–0.67 is an interstellar bubble powered by the stellar winds of HD 24431. The origin of SH 149.25–0.00, which can hardly be distinguished by its optical and faint radio emission, remains an open question since no stellar object was found associated with the nebula. The shell centred at $(l, b) = (149°0', -1°30')$, of $\approx 2°2 \times 1°5$ in size, is placed at a kinematical distance of 1.5 kpc and may be related to the open cluster NGC 1444.

The most striking area is LBN 148.11–0.45. This is a classical H II region of $30 \times 24 \, \mathrm{arcmin}^2$ in size and $4 \times 10^6 \, \mathrm{yr}$ in age. Neutral atomic and molecular gas in the velocity range [−0.65, −11.1] km s^{-1} partially encircles this ionized region. It is also closely surrounded by a dust ring detected in the mid- and far-infrared, suggesting the presence of a photodissociation region (PDR) at the interface between the ionized and molecular regions. The derived ambient density ($n_o \approx 800 \, \mathrm{cm}^{-3}$) indicates that this H II region is evolving in a dense interstellar medium (Paper I).

The morphology of this H II region encouraged us to look for signposts of star-formation activity at its periphery. In this paper we

★E-mail: gisela@dfa.uv.cl
†Post-doctoral fellow of Universidad de Valparaíso, Chile.
‡Member of the Carrera del Investigador Científico of CONICET, Argentina.
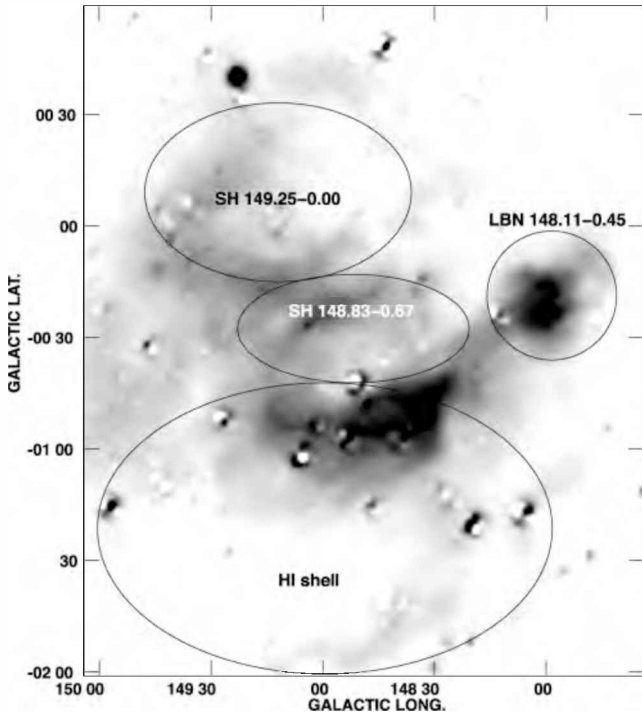
Figure 1. Overview of the Sh2-205 region: the areas discussed in the paper are schematically indicated in the VTSS continuum image.

investigate the star-formation activity in the three different structures of Sh2-205 and in the large H i shell, based on infrared point source catalogues.

The present paper is organized as follows: Section 2 gives a brief description of the methods we used to find tracers of star-formation activity, while Section 3 shows the main results obtained for the four analysed regions: LBN 148.11–0.45, SH 148.83–0.67, SH 149.25–0.00 and the H i shell. Whether our findings are compatible with the collect and collapse process is discussed in Section 4. A summary of the main results is presented in Section 5.

2 DATA SETS AND SELECTION CRITERIA

In order to find primary indicators of star-formation activity in the region under study, we used the MSX6C Infrared Point Source Catalogue (Egan et al. 2003) in bands A (8.3 μm), C (12.1 μm), D (14.7 μm) and E (21.3 μm); the Two Micron All-Sky Survey (2MASS) Point Source Catalogue (Cutri et al. 2003) in bands *J* (1.25 μm), *H* (1.65 μm) and *Ks* (2.17 μm); and the *IRAS* Point Source Catalogue.[1] In addition, broad-band mid- and far-infrared data supplied by the *Midcourse Space Experiment (MSX)* and *IRAS* satellites were employed to show the large-scale distribution of the dust. Star-formation activity was investigated within a box centred at $(l, b) = (148°45', -0°45')$, of side $2°.5$.

^{12}CO(1—0) data from Dame, Hartmann & Thaddeus (2001) were also used to compare the spatial distribution of the tracers of star-formation activity with that of the molecular gas. These data have an angular resolution of 8.3 arcmin, a velocity resolution of 1.3 km s^{-1}, and an rms noise of 0.05 K.

The criteria used to identify YSO candidates are described in the following paragraphs.

^{1} 1986 *IRAS* catalogue of Point Sources, Version 2.0 (II/125).

2.1 *IRAS* sources

A total of 89 *IRAS* point sources were found projected on to the analysed region. Junkes, Fürst & Reich (1992)'s conditions for young stellar objects are as follows: $S_{100} \geq 20\,\mathrm{Jy}$, $1.2 \leq S_{100}/S_{60} \leq 6.0$, $S_{100}/S_{60} \geq 1$ and $Q_{60} + Q_{100} \geq 4$, where S_λ and Q_λ are the flux density and the quality of the *IRAS* fluxes in each of the observed bands, respectively. Only seven of the 89 sources can be classified as protostellar candidates following the above-mentioned criteria.

2.2 *MSX* sources

The sources were classified based on Lumsden et al. (2002)'s criteria, which allow one to select sources taking into account their loci in the $(F_{21}/F_8, F_{14}/F_{12})$ diagram. F_λ denotes the flux in each band. Massive young stellar object (MYSO) candidates have $F_{21}/F_8 \gtrsim 2$ and $F_{14}/F_{12} \gtrsim 1$, while compact H ii regions (CHII) present $F_{21}/F_8 \gtrsim 2$ and $F_{14}/F_{12} < 1$. Evolved stars occupy the region $F_{21}/F_8 \leq 2$ and $F_{14}/F_{12} \leq 1$.

A total of 128 *MSX* sources are projected on to the whole region. Most of the sources are detected only in the highest sensitivity band A, while 4 per cent of the sources are detected in band E. For the case of bands C and D, 15 per cent of the sources reach the detection limit of the instrument. Of the detected sources, 20 per cent and 33 per cent have reliable fluxes (corresponding to quality flags 3 or 4) in bands C and D, and B and E, respectively. Only the sources detected in bands A and E are included in the present analysis. Among the sources with reliable fluxes, only one can be catalogued as a MYSO candidate. Another two sources, which are not detected in band C, can be classified as young stellar objects, but their identification as MYSOs or CHII remains uncertain.

2.3 2MASS sources

A total of 6548 sources were selected from the 2MASS catalogue. These sources have a photometric quality Qflg = AAA.[2] Mean errors are 0.024, 0.03 and 0.023 mag for *J*, *H* and *Ks* magnitudes, respectively. The nature of the sources can be inferred from their position in the $(H - Ks, Ks)$ colour–magnitude (CM) and $(H - Ks, J - H)$ colour–colour (CC) diagrams. Following Comerón & Pasquali (2005), we define the parameter q as

$$q = (J - H) - 1.83 \times (H - Ks). \tag{1}$$

This parameter allows identification of sources in different evolutionary stages. Main-sequence stars have q values in the range -0.15 to 0.10, while sources with infrared excess, like YSOs, have $q \lesssim -0.15$. For giant stars, $q \gtrsim 0.10$.

The selection criteria described above were applied to the Sh2-205 area and to a control field. The latter is centred at $(l, b) = (146°45', -0°45')$ and is $2°.5 \times 2°.5$ in size. We believe its stellar population is dominated by field stars. Fig. 2 shows the CC (upper left panel) and CM (bottom panel) diagrams for main-sequence star candidates and sources with infrared excess found towards Sh2-205. The CC diagram of the control field is presented in the upper right panel of Fig. 2. The reddening vectors for early type
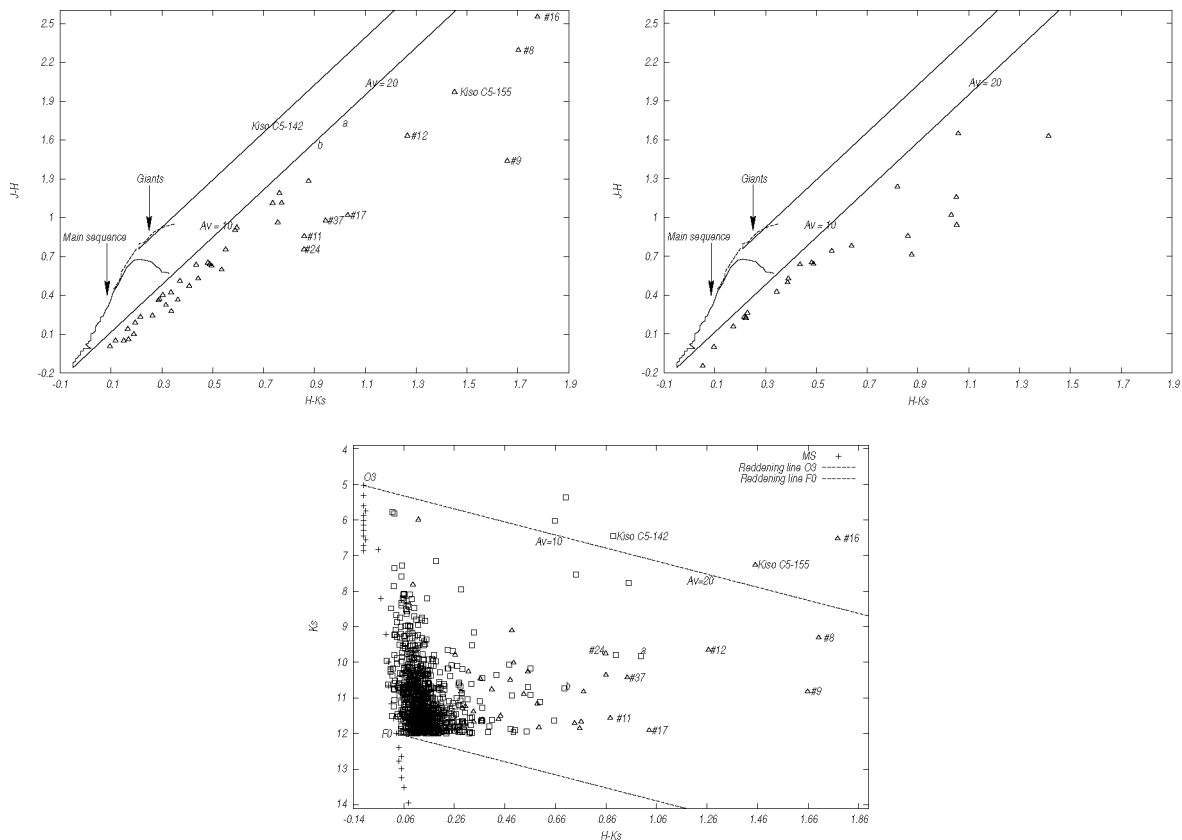
Figure 2. CC and CM diagrams of the 2MASS sources towards Sh2-205 and the control area. YSO and main-sequence star candidates are indicated by triangles and squares, respectively. Upper panels: ($H − Ks$, $J − H$) diagram of Sh2-205 (left panel) and a control field (right panel). The locations of the de-reddened early-type main-sequence and giant stars are shown. The reddening curves for M0 III stars (upper line) and O6–8 V stars (lower line) are indicated. Lower panel: (Ks, $H − Ks$) diagram. The crosses mark the position of the main sequence without extinction at a distance of 1.0 kpc (Tokunaga 2000; Drilling & Landolt 2000; Martins & Plez 2006). The reddening curves for an O3 and a F0 star are shown with dashed lines. Sources with high infrared excess have been identified by the corresponding numbers and letters.

(O6–8 V) and late-type (M0 III) stars (Koornneef 1983) are represented by two parallel lines in the CC diagrams using extinction values from Rieke & Lebofsky (1985). The position of the main sequence at a distance of 1.0 kpc is indicated by the crosses in the ($H − Ks$, Ks) diagram.

Towards Sh2-205 we found 41 sources with infrared excess (triangles in Fig. 2), 1082 main-sequence stars (represented by squares in the CM diagram of Fig. 2) and 5425 giant stars (not included in the plot). In the CC diagram corresponding to Sh2-205, several sources located just below the reddening curve for an O6–8 V star, with q values close to 0.1 (not shown in the plot), were included as main-sequence star candidates. As regards the control field, we found 23 sources with infrared excess, around half the number identified towards Sh2-205. These sources did not show any spatial clustering. In contrast, some spatial clustering was found toward Sh2-205 (see Section 3). We note that some of the sources with infrared excess that are situated very close to the reddening vector, especially at low extinctions, might be early-type stars with small photometric errors, moderate deviations of the actual reddening law from the adopted one or intrinsic scatter in the colours of early-type stars. If this were the case, the diagram would be indicating an excess of early-type stars, probably related to the H II region. The condition for Ks magnitudes causes a region lacking sources in the CM diagram between $Ks = 12$ and the reddening curve for a F0 star, thus underestimating the number of Herbig Ae/Be candidates in the analysed region.

The CC diagram shows a group of four main-sequence star candidates that have the highest values of visual extinction ($A_v \approx 15$ mag). The one named Kiso C5-142 in the Simbad data base, with values ($H − Ks$, $J − H$) = (0.89, 1.71), and the source with high infrared excess named Kiso C5-155, with ($H − Ks$, $J − H$) = (1.47, 1.97), are actually carbon stars (Alksnis et al. 2001). The nature of the other two main-sequence star candidates will be discussed in the following section.

3 DISTRIBUTION OF YSOS

In this section, we will examine the spatial distribution of the detected YSO candidates.

Fig. 3 shows an overlay of the ^{12}CO emission distribution in the velocity range [−0.65, −11] km s^{-1} (left panel) and the 1420-MHz image (right panel) and the probable tracers of star-formation activity. *IRAS, MSX* and 2MASS candidates are indicated as crosses, circles and triangles, respectively. To associate an infrared source with a certain H II region or interstellar bubble within the area under study, we considered its proximity to the structure and its correlation with the neutral/ionized associated gas. We are aware of the fact that no distance information is available in most of the cases. The condition $Ks < 12$ for the 2MASS sources implies an upper limit to the distance of the sources. The adopted Ks value indicates that we can see an O3-type star with $A_v \approx 60$ mag and a B5-type star with $A_v \approx 20$ mag at a distance of 1.0 kpc. We discuss our results for the
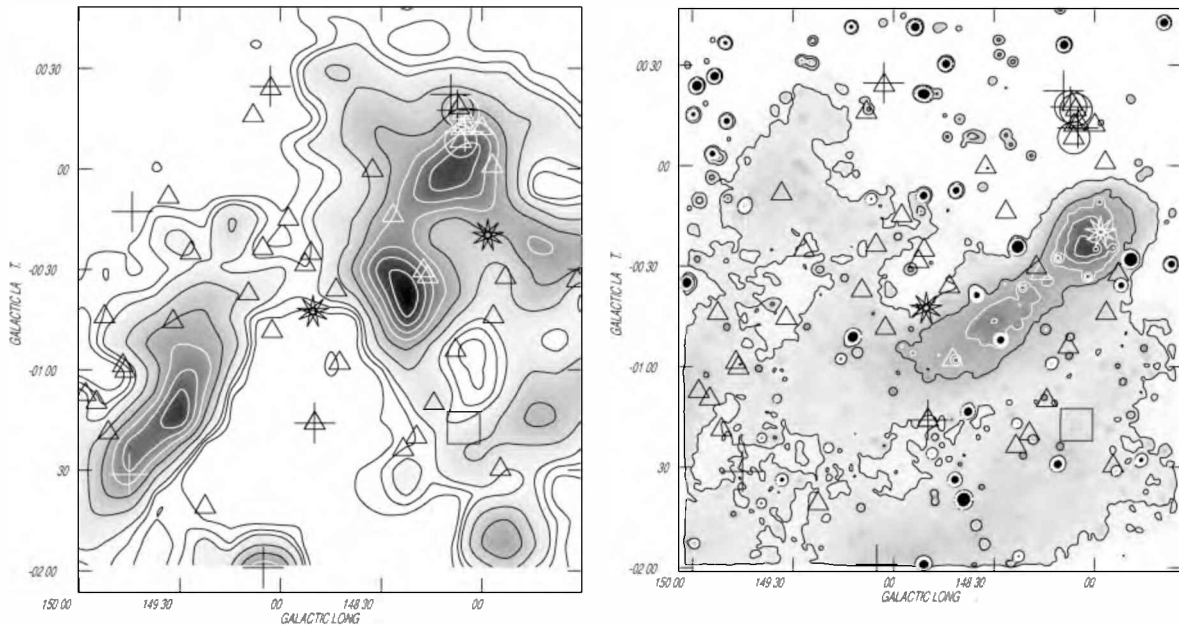
Figure 3. Left panel: YSO candidates superimposed on to the molecular emission averaged within the velocity range $[-0.65, -11.1]\,\mathrm{km\,s^{-1}}$. Contour levels are 0.5, 1.0, 1.5 K, and from 3–15 K in steps of 2 K. Right panel: YSO candidates superimposed on to the emission at 1420 MHz. Contour levels are from 5.3–6.1 K in steps of 0.2 K. 2MASS, *IRAS* and *MSX* candidates are indicated by triangles, crosses and circles, respectively. HD 2431 and HD 24094 are identified by nine pointed stars. The box indicates the position of NGC 1444.

four regions – LBN 148.11–0.45, SH 148.83–0.67, SH 149.0–1.30 and the H I shell – separately.

3.1 Star formation in LBN 148.11–0.45

The distribution of gas and dust in the environs of LBN 148.11–0.45 is shown in Fig. 4. The left panel shows the YSO candidates in the environs of LBN 148.11–0.45 superimposed on the emission at 8.3 μm. Numerous infrared objects are seen projected on to this region. 2MASS, *IRAS* and *MSX* candidates are indicated by triangles, crosses and circles, respectively.

The top right panel displays an overlay of the ^{12}CO(1–0) emission distribution (*contours*) in the range $[-0.65, -11.1]\,\mathrm{km\,s^{-1}}$ and the infrared emission at 100 μm (*grey-scale*), while the bottom right panel depicts an overlay of the ^{12}CO(1–0) emission distribution (*contours*) in the range $[-31.9, -35.8]\,\mathrm{km\,s^{-1}}$ and the 100 μm image.

Properties of *IRAS*, *MSX* and 2MASS sources are listed in Table S1. The designation of the *IRAS* sources, (l, b) positions, fluxes at 12, 25, 60 and 100 μm, luminosities derived following Yamaguchi et al. (1999) and association with other sources, along with a reference number, are indicated in the table. For the *MSX* sources we included the candidate designation, the (l, b) position, the fluxes at 8.3, 12.1, 14.7 and 21.3 μm, and the association with other sources. The quality flag of the sources in each band, Q_{flag}, is indicated in column 8 by a number from 0 to 4. While '0' means that the source has not been detected, '1' to '4' indicate a better detection of the source as the number increases. Identification as MYSO or CHII is included. As regards 2MASS candidates, names, (l, b) positions, fluxes in the 2MASS infrared wavelengths, colours $(J - H)$ and $(H - Ks)$ and association with other sources are listed.

This region can be divided into two areas based on the distribution of the YSO candidates: one close to $(l, b) = (148°, +0° 15')$ and the other near LBN 148.11–0.45 itself (see Fig. 4).

12 candidates are projected near $(l, b) = (148°, +0° 15')$. An inspection of the image at 100 μm shows that the candidates coincide with filamentary emission. This extended feature is not detected at 8.3 μm. At this wavelength, only knots of bright emission coincident with the sources are identified.

The YSO candidates are found projected on to the molecular cloud detected in the velocity range $[-31.9, -35.8]\,\mathrm{km\,s^{-1}}$ (see Fig 3, bottom right panel). The source IRAS 03523+5343 (*IRAS* #2) was associated with molecular gas detected in ^{12}CO at $v = -34.6\,\mathrm{km\,s^{-1}}$ by Wouterloot & Brand (1989), who derived a kinematical distance $d_k \approx 4.2\,\mathrm{kpc}$. Adopting this distance, the infrared luminosity of the source is $6500\,\mathrm{L}_\odot$ (Yamaguchi et al. 1999). One can speculate whether this star-forming region might be an outflow of the H II region LBN 14811–0.45, and consequently be placed at the same distance. The presence of molecular emission with velocities in the range $[-0.65, -11.1]\,\mathrm{km\,s^{-1}}$ bordering the ionized region at $b = -0° 10'$ casts doubts on this interpretation. On the other hand, if the molecular cloud at $-34\,\mathrm{km\,s^{-1}}$ were located at the distance of the H II region then this cloud would have an approaching velocity of at least $25\,\mathrm{km\,s^{-1}}$, while we would expect a radial velocity closer than the systemic velocity of the H II region for a champagne flow. Moreover, radio emission from the ionized gas in the region between LBN 14811–0.45 and the star-forming area, which should be present in a champagne flow, is absent.

IRAS 03529+5345 (*IRAS* #1) is almost coincident in position with a nebular object present in the National Geographic Society–Palomar Observatory (NGS–PO) Sky Survey and called RNO22 by Cohen (1980), who established from an optical spectrum that it was an F5 star, with relatively high reddening. Based on this classification and the apparent magnitude $m_v = 15.3\,\mathrm{mag}$ and visual extinction given by the author, and taking into account $M_v = 3.5\,\mathrm{mag}$ (Drilling & Landolt 2000), we estimated a distance of $\approx 500\,\mathrm{pc}$ for the F5 star. On the other hand, a chance superposition cannot be ruled out. Moreover, the presence of other evidence of active star formation 4 arcmin away from *IRAS* #1, and located at
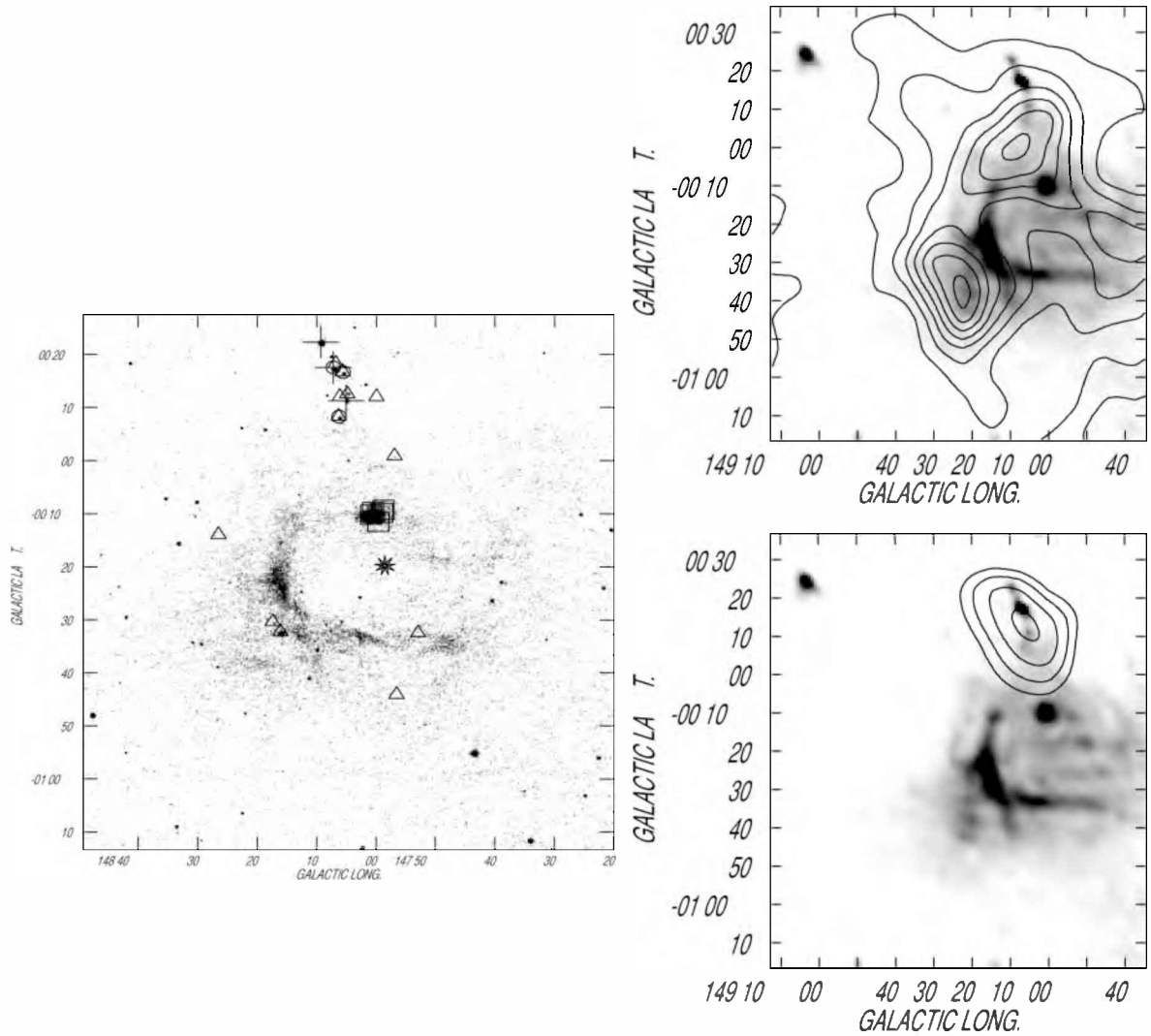
Figure 4. Left panel: image at 8.3 µm. YSO candidates from 2MASS, *IRAS* and *MSX* sources are indicated by triangles, crosses and circles, respectively. HD 24094 is identified by a nine-point star. Main-sequence candidates are indicated by squares. Top right panel: 100 µm image (grey-scale) and ^{12}CO emission distribution (contours) within the velocity range $[-0.65, -11.1]$ km s^{-1}. Contour levels are 1.0 K, 1.5 K, and from 2.0–6.0 K in steps of 1 K. Bottom right panel: overlay of the 100 µm image (grey-scale) and ^{12}CO emission distribution (contours) within the velocity range $[-31.9, -35.8]$ km s^{-1}. Contour levels are from 1.0–2.5 K in steps of 0.5 K.

larger distances, casts doubts on the association of the *IRAS* source and the F5 star.

As regards IRAS 03517+5340 (*IRAS* #3), no additional information is found in the literature. It is also probably related to molecular gas at -33 km s^{-1}. If it is located at 4.2 kpc, its infrared luminosity also suggests a massive object.

MSX sources #4 and #5 and 2MASS sources #7 and #8 are almost coincident with *IRAS* #2, while 2MASS sources #9 and #11 are projected on to the position of *IRAS* #3. *MSX* source #6 and 2MASS source #12 are close to the last group. Note that #8, #9 and #12 are among the sources with the highest infrared excess (see Fig. 2). Source #10 is also probably connected to the star-forming region at $d \approx 4.2$ kpc.

As regards, LBN 148.11–0.45, the 2MASS sources #13–#18 are placed close to the ionized border. They are projected on to the molecular structure detected within the range $[-0.65, -11.1]$ km s^{-1}. Sources #13, #14, #16 and #18 appear projected on to the outer border of the PDR, marked by the emission at 8.3 µm (see Fig. 4, left and top right panels).

The 2MASS source #16 has the highest infrared excess in the region $[(H - Ks, J - H) = (1.78, 2.55)]$. It is projected on to the PDR, close to the brightest CO emission region. No additional information on the 2MASS YSO candidates is found in the literature.

The *MSX* knot at $(l, b) = (148°0', -0°10')$ is an interesting object. As found in Paper I, it is 1.5 arcmin away from the radio continuum point source NVSS J035327+533601, which is a non-thermal, probably extragalactic source. Flux densities for this source are 45 ± 27 mJy and 13 ± 0.9 mJy at 408 MHz and 1420 MHz, respectively, and the spectral index is -1.00 ± 0.2 (Paper I). A total of five main-sequence candidates are projected on to this knot of emission. They are listed in the bottom part of Table S1. Sources #a and #b have the highest visual extinction among the complete set of main-sequence stars. It would be interesting to investigate the true nature of this object.

The difference in distance between the H II region LBN 148.11–0.45 and *IRAS* #2 and #3 suggests that we have identified two independent star-forming regions, without apparent physical relation. *IRAS* #1 is a late-type star seen projected on to the environs of
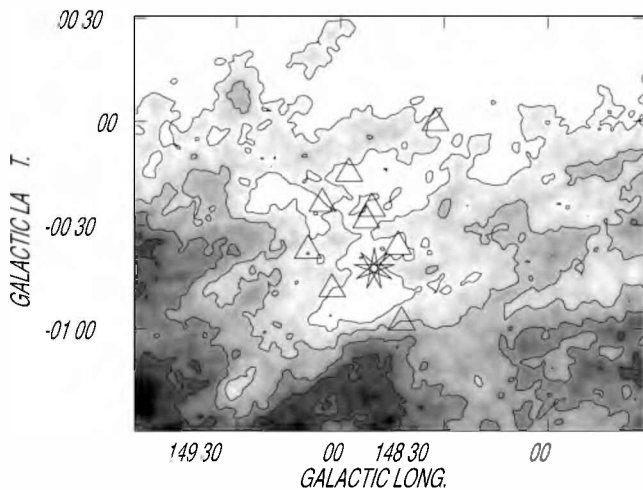
Figure 5. YSO candidates superimposed on to the atomic neutral gas emission distribution associated with SH 148.83–0.67. The map shows the H I emission distribution in the velocity range from −25.0 to −28.0 km s^{-1}. Contour levels are from 60–100 K in steps of 10 K. 2MASS candidates are indicated by triangles. HD 24431 is identified by a nine-pointed star.

LBN 148.11–0.45, without physical association with either the H II region or the star-forming area at 4.2 kpc.

To sum up, we have identified two star-forming regions: one near $(l, b) = (148°0', +0°15')$ and the other connected to LBN 148.11–0.45.

As regards the first area, placed at $d \approx 4.2$ kpc, 11 primary tracers were identified. Six YSO candidates were found in the environs of LBN 148.11–0.45, most of them located in the PDR.

3.2 Star formation in SH 148.83–0.67 and SH 149.25–0.00

Protostellar objects associated with this region are listed in Table S2, which is organized in the same way as Table S1. Fig. 3 shows several 2MASS candidates projected on to the radio continuum emission at 1420 MHz. No *IRAS* and *MSX* candidates are found in this region.

Eight YSO candidates were found in this region. Fig. 3 shows the spatial distribution of the candidates on to the atomic neutral gas structure associated with SH 148.83–0.67 (Paper I). This figure shows the 21-cm H I line emission within the velocity range [−25.0, −28.0] km s^{-1} (Paper I). Source #26 coincides with the radio continuum point source NVSS J035347+523208, which is probably a pulsar. Flux densities for this source are 33 ± 16 mJy and 1.94 ± 0.25 mJy at 408 and 1420 MHz, respectively. The spectral index is −2.27 ± 0.68 (Paper I).

To summarize, the 2MASS sources are projected on to the H I low-emission region and are characterized by low infrared excess, compatible with the lack of related molecular and dust emission. This fact casts doubt on the nature of the sources. 2MASS sources #20 and #23 (see Table S2) coincide with HBHA 5215-03 and HBHA 5215-01, two emission-line stars (Kohoutek & Wehmeyer 1999). No additional data for these sources are found in the literature.

As regards SH 149.25–0.00, five 2MASS and one *IRAS* candidate were found in this region (Table S3). *IRAS* source #27 is associated with DSH J0402.3+5226. This source was identified as an infrared cluster by Kronberger et al. (2006), reinforcing its identification as a star-formation tracer. YSO candidates associated with this nebula are listed in Table S3, where the information is organized as in

Table S1. Additional data for these sources were not found in the literature.

In summary, eight candidates were found towards SH 148.83–0.67, and six were identified towards SH 149.25-0.00. The lack of molecular gas linked to these sources strengthens the uncertainty regarding their true nature.

3.3 Star formation in the H I shell centred at $(l, b) = (149°0', -1°30')$

Based on the criteria mentioned in Section 3, two *IRAS* and eight 2MASS candidates are projected on to the environs of the H I and CO shells. They are listed in Table S4.

Source #34 was associated with the reflection nebula GN 03.53.0 by Magakian (2003).

IRAS source #33 was identified by Campbell, Persson & Matthews (1989) as a YSO candidate based on its colours $(H - Ks, J - H)$. Its near-infrared counterpart is 2MASS #37. Its distance is unknown. This source is projected on to the void of molecular emission, suggesting that this object is unconnected to the H I shell.

2MASS sources #38 and #41, which are projected close to the inner border of the molecular ring, were identified as the near-infrared counterpart of HD 23800 (B1.5 IVe, Hiltner 1956) and HD 24275 (A3 V, Rydstrom 1978), respectively. These sources have low infrared excess and lie in the bottom left section of the $(H - Ks, J - H)$ diagram (Fig. 2), where objects in different evolutionary stages are found (Lada & Adams 1992).

There is a group of six 2MASS sources with $l \leq 149°$ 30' (see Fig. 3), which are projected on to the outer border of the molecular ring. These sources may be a connected to Sh2-206, located at $(l, b) = (150°36'.18, -00°56'.52)$, of 50 arcmin in diameter. Sh2-206 is a blister H II region catalogued as a star-forming region (Mookerjea et al. 1999). Up to the present, neither a near- nor a mid-infrared systematic study has been performed to search for star-formation tracers in this region. However, the positions of these 2MASS sources suggest that they may be associated with Sh2-206.

To sum up, five YSO candidates probably related to the H I and CO shell were identified.

4 DISCUSSION

MSX emission at 21.3 μm is essential to detect embedded sources in molecular clouds (e.g Rathborne et al. 2004). However, the low sensitivity in band E makes it difficult to detect sources at 21.3 μm. This fact leads us to underestimate the number of *MSX* point sources, since only sources detected in both bands A and E have been taken into account. Additionally, only 20–30 per cent of the YSOs can be identified by using 2MASS CC and CM diagrams, as Nielbock, Chini & Müller (2003) found in the star-forming regions OMC 2 and 3. As a consequence, the number of candidates in our analysed regions is underestimated.

Taking into account these constraints, LBN 148.11–0.45 shows a notably interesting scenario. The YSO candidates are found in the periphery of the optical nebula, on or close to the PDR and embedded in the molecular gas. Additionally, the age of the H II region (4 × 10^6 yr, Paper I) is compatible with the existence of Class I sources (André & Motte 2000).

This H II region is evolving in an interstellar medium with an original ambient density of ≈800 cm^3 (Paper I). These results open the question of whether this region is another example of triggered star formation in our Galaxy. The 'collect and collapse' model indicates that the expansion of H II regions into their surroundings

creates compressed layers where gas and dust are piled up between the ionization and shock fronts. The latter fragmentation of the collected layer ends, forming molecular cores where new stars are born. The analytical model developed by Whitworth et al. (1994) analysed the consequences of the dynamical instabilities occurred in the collected layer. They considered three different scenarios where the fragmentation can occur: expanding H II regions, stellar wind bubbles and supernova remnants. In all cases, they found that the resulting fragmentation in the shocked layers generates high-mass clumps (i.e. $\geq 7\,M_\odot$), which are initially well separated.

For the case of H II regions, the theory predicts the time at which the fragmentation occurs, t_{frag}, the size of the H II region at that moment, R_{frag}, the column density of the shell when the process begins, N_{frag}, the mass of the fragments, M_{frag}, and their separation along the layers, r_{frag}. The parameters required to derive these quantities are the number of Lyman continuum photons emitted per second by the exciting sources, N_{Ly}, the ambient density of the surrounding medium into which the H II region expands, n_0, and the isothermal sound speed in the shocked gas, a_{s}, which is supposed to be constant.

The analytical expressions are

$$t_{\mathrm{frag}}[10^6\mathrm{yr}] = 1.56 a_{.2}^{4/11} n_3^{-6/11} N_{\mathrm{Ly}}^{-1/11}, \tag{2}$$

$$R_{\mathrm{frag}}[\mathrm{pc}] = 5.8 a_{.2}^{4/11} n_3^{-6/11} N_{\mathrm{Ly}}^{1/11}, \tag{3}$$

$$N_{\mathrm{frag}}[10^{21}\mathrm{cm}^{-2}] = 6.0 a_{.2}^{4/11} n_3^{-6/11} N_{\mathrm{Ly}}^{1/11}, \tag{4}$$

$$M_{\mathrm{frag}}[\mathrm{M}_\odot] = 23 a_{.2}^{40/11} n_3^{-5/11} N_{\mathrm{Ly}}^{-1/11}, \tag{5}$$

$$2r_{\mathrm{frag}}[\mathrm{pc}] = 0.83 a_{.2}^{18/11} n_3^{-5/11} \mathrm{N}_{\mathrm{Ly}}^{-1/11}, \tag{6}$$

where $a_{.2} \equiv a_{\mathrm{s}}/(0.2\,\mathrm{km\,s}^{-1})$ and $n_3 \equiv n_0/(1000\,\mathrm{cm}^3)$.

These equations show that a_{s} is an important factor in deriving the parameters, while n_0 has a lower contribution, and the dependence on N_{Ly} is notoriously weak. A remarkable result from equation (5) is that the mean mass of the fragments increases as the sound speed grows.

For the case of LBN 148.11–0.45, the parameters N_{Ly} and n_0 were derived from the free–free radio continuum emission (Paper I). The rate of Lyman continuum photon emission is at least $4 \times 10^{47}\,\mathrm{s}^{-1}$, and the ambient density $800\,\mathrm{cm}^3$. Whitworth et al. (1994) pointed out that a_{s} is in the range from 0.2–0.6 km s^{-1}. For this H II region, the larger a_{s} values lead to unrealistic parameters. For example, for $a_{\mathrm{s}} = 0.35\,\mathrm{km\,s}^{-1}$, the mass of the fragments increases dramatically ($\approx 300\,\mathrm{M}_\odot$) and their radii reach values larger than the size of the H II region. Acceptable parameters are obtained for the present case by taking into account a_{s} in the range 0.2–0.3 km s^{-1}. In the following, we will adopt a value of 0.2 km s^{-1}, which corresponds to a typical temperature of 10 K for the molecular clouds.

Considering that the radius of the H II region is $R_{\mathrm{H\,II}} = 7.2\,\mathrm{pc}$, and the dynamical age $t_{\mathrm{dyn}} = 4 \times 10^6\,\mathrm{yr}$, we compare them with the derived parameters (Table 1). According to the table, $R_{\mathrm{frag}} < R_{\mathrm{H\,II}}$ and $t_{\mathrm{dyn}} > t_{\mathrm{frag}}$, indicating that massive molecular fragments were able to form in the environs of LBN 148.11–0.45. The distance between fragments is lower than the minimum linear size that the angular resolution of CO data allows us to separate (i.e. $r = 2.4\,\mathrm{pc}$ at a distance of 1.0 kpc). Better angular resolution data and different line transitions are needed to observe the molecular fragments. Other phenomena of fragmentation can act simultaneously in this zone. Molecular cores can be formed by radiative-driven collapse, namely

Table 1. Parameters for the the shocked layers in the environs of LBN 148.11–0.45.

Parameter	Value
M_{frag} [M$_\odot$]	33
t_{frag} [10^6 yr]	2.3
R_{frag} [pc]	5
r_{frag} [pc]	0.6
N_{frag} [10^{21} cm^{-2}]	4

the so-called 'radiation-driven implosion' (RDI) theoretically developed by Lefloch & Lazareff (1994). Structures such as cometary globules and elephant trumps can be observational examples of this process (e.g. Lefloch, Lazareff & Castets 1997). However, the angular resolutions of optical and infrared observations do not allow us to identify the presence of these objects. As a consequence, there is neither evidence nor necessary data to apply the RDI model in this region. Thus, neither of the two models can be discarded to explain the star-formation process in the environs of LBN 148.11–0.45.

5 SUMMARY

We have analysed the star-formation activity in four different regions of Sh2-205.

Based on *MSX*, 2MASS and *IRAS* point source catalogues, we have identified YSO candidates in the region by applying criteria by Junkes et al. (1992), Lumsden et al. (2002) and using CM and CC diagrams. Additional information was obtained from the Simbad data base and broad-band mid- and far-infrared images supplied by the *MSX* and *IRAS* satellites, and ^{12}CO(1—0) data.

Our main results can be summarized as follows.

(1) Six of the seven *IRAS*, 30 of the 41 2MASS and the three *MSX* sources identified as YSO candidates were found projected on to the four structures.

(2) Of these, eight candidates were found towards SH 148.83–0.67, and six candidates were identified towards SH 149.25-0.00. However, the lack of molecular gas linked to these sources casts doubt on their nature and their physical association with the structures.

(3) Five YSO candidates probably related to the H I and CO shell centred at $(l, b) = (149°0', -1°30')$ were identified. The agent responsible for this structure remains unknown.

(4) In the environs of LBN 148.11–0.45 we have identified two star-forming regions: one near $(l, b) = (148°0', +0°15')$ and the other connected to LBN 148.11–0.45 itself.

As regards the first area, placed at $d \approx 4.2\,\mathrm{kpc}$, eleven primary tracers were identified.

Six YSO candidates were found in the environs of LBN 148.11–0.45. Most of them are situated close to the PDR, projected on to molecular material. By applying Whitworth et al. (1994)'s theoretical model to this region, we find that the formation of massive fragments would be taking place in this region. Higher angular resolution data are necessary to detect the molecular fragments.

(5) Finally, two findings can be highlighted: the presence of tracers of star-formation activity found in LBN 148.11–0.45 and the requirement of high UV photon flux necessary to keep this H II region ionized. The combination of these two reinforces the argument that HD 24094 was misclassified as a B8-type star (Paper I) and the existence of hidden exciting sources responsible for this star-formation process.

6 FUTURE WORK

Millimetre observations are needed to confirm whether fragmentation is occurring in the environs of LBN 148.11–0.45. Near- and mid-infrared data are important to detect the embedded sources. The *Spitzer* satellite is much more sensitive and has higher spatial resolution than the infrared surveys used in this work (Werner et al. 2004). In particular, IRAC and MIPS 24 μm colour–colour diagrams ([3.6]–[5.8], [8.0]–[24.0]) provide a good observational tool for determining the evolutionary stage of YSOs (Robitaille et al. 2006). Unfortunately, no *Spitzer* data are available for this region. High-quality *Spitzer* data would allow a more accurate and comprehensive analysis of star-formation activity in the environs of LBN 148.11–0.45.

REFERENCES

Alksnis A., Balklavs A., Dzervitis U., Eglitis I., Paupers O., Pundure I., 2001, Baltic Astron., 10, 1
André P., Motte F., 2000, in Favata F., Kaas A., Wilsoneds A., eds, ESA Spec. Pub. Vol. 445, Proc. ESLAB Symp. 33, Star Formation from the Small to the Large Scale. ESA, Noordwijk, p. 219
Campbell B., Persson S. E., Matthews K., 1989, AJ, 98, 643
Cappa C., Niemela V. S., Martín M. C., McClure-Griffiths N. M., 2005, A&A, 436, 155
Cohen M., 1980, AJ, 85, 29
Comerón F., Pasquali A., 2005, A&A, 430, 541
Cutri R. M. et al., 2003, The IRSA 2MASS All-Sky Catalog of Point Sources, NASA/IPAC Infrared Science Archive http://irsa.ipac.caltech.edu/applications/Gator
Dale J. E., Bonnell I. A., Whitworth A. P., 2007, MNRAS, 375, 1291
Dame T. M., Hartmann D., Thaddeus P., 2001, ApJ, 547, 792
Deharveng L., Zavagno A., Caplan J., Lefloch B., Salas L., Porras A., Cruz-González I., 2003, A&A, 408, L25
Deharveng L., Zavagno A., Caplan J., 2005, A&A, 433, 565
Drilling J. S., Landolt A. U., 2000, in Cox A. N., ed., Allen's Astrophysical Quantities, 4th edn. Am. Inst. Phys., New York, p. 381
Egan M. P. et al., 2003, The Midcourse Space Experiment Point Source Catalog Version 2.3 (October 2003) Air Force Research Laboratory Technical Report AFRL-VS-TR-2003-1589 (V/114)
Elmegreen B. G., Lada C. J., 1977, ApJ, 214, 725
Hiltner W. A., 1956, ApJS, 2, 389
Junkes N., Fürst E., Reich W., 1992, A&A, 261, 289
Kohoutek L., Wehmeyer R., 1999, A&AS, 134, 255
Koornneef J., 1983, A&A, 128, 84
Kronberger M. et al., 2006, A&A, 447, 921
Lada C. J., Adams F. C., 1992, ApJ, 393, 278
Lefloch B., Lazareff B., 1994, A&A, 289, 559
Lefloch B., Lazareff B., Castets A., 1997, A&A, 324, 249
Lumsden S. L., Hoare M. G., Oudmaijer R. D., Richards D., 2002, MNRAS, 336, 621
Magakian T. Y., 2003, A&A, 399, 141
Martins F., Plez B., 2006, A&A, 457, 637
Mookerjea B., Ghosh S. K., Karnik A. D., Rengarajan T. N., Tandon S. N., Verma R. P., 1999, ApJ, 522, 285
Nielbock M., Chini R., Müller S. A. H., 2003, A&A, 408, 245
Rathborne J. M., Brooks K. J., Burton M. G., Cohen M., Bontemps S., 2004, A&A, 418, 563
Rieke G. H., Lebofsky M. J., 1985, ApJ, 288, 618
Robitaille T. P., Whitney B. A., Indebetouw R., Wood K., Denzmore P., 2006, ApJS, 167, 256
Romero G. A., Cappa C. E., 2008, MNRAS, 387, 1080 (Paper I)
Rydstrom B. A., 1978, A&AS, 32, 25
Tokunaga A. T., 2000, in Cox A. N., ed., Allen's Astrophysical Quantities, 4th edn. Am. Inst. Phys., New York, p. 143
Werner M. W. et al., 2004, ApJS, 154, 1
Whitworth A. P., Bhattal A. S., Chapman S. J., Disney M. J., Turner J. A., 1994, MNRAS, 268, 291
Wouterloot J. G. A., Brand J., 1989, A&AS, 80, 149
Yamaguchi R., Saito H., Mizuno N., Mine Y., Mizuno A., Ogawa H., Fukui Y., 1999, PASJ, 51, 791
Zavagno A., Deharveng L., Comerón F., Brand J., Massi F., Caplan J., Russeil D., 2006, A&A, 446, 171

SUPPORTING INFORMATION

Additional Supporting Information may be found in the online version of this article:

Table S1. YSO candidates from the *IRAS*, *MSX* and 2MASS catalogues towards LBN 148.11–0.45.
Table S2. YSO candidates from the 2MASS catalogue towards SH 148.83–0.67.
Table S3. YSO candidates from the *IRAS* and 2MASS catalogues towards SH 149.25–0.00.
Table S4. YSO candidates from the 2MASS catalogue towards H I shell centred at $(l, b) = (149°0', -1°30')$.

Please note: Wiley-Blackwell are not responsible for the content or functionality of any supporting materials supplied by the authors. Any queries (other than missing material) should be directed to the corresponding author for the article.

This paper has been typeset from a TEX/LATEX file prepared by the author.